Scientific Research Publishing

Open Journal of Applied Sciences, 2024, 14, 1165-1184
https://www.scirp.org/journal/ojapps
ISSN Online: 2165-3925
ISSN Print: 2165-3917

# Phase-Based Optical Flow Method with Optimized Parameter Settings for Enhancing Displacement Measurement Adaptability

**Zhaoxin Peng, Menglian Liu, Zhiliang Wang, Wei Liu, Xian Wang**

School of Mechanical Engineering, Hunan University of Science and Technology, Xiangtan, China
Email: p851542000@gmail.com

**How to cite this paper:** Peng, Z.X., Liu, M.L., Wang, Z.L., Liu, W. and Wang, X. (2024) Phase-Based Optical Flow Method with Optimized Parameter Settings for Enhancing Displacement Measurement Adaptability. *Open Journal of Applied Sciences*, **14**, 1165-1184.
https://doi.org/10.4236/ojapps.2024.145075

**Received:** March 28, 2024
**Accepted:** May 3, 2024
**Published:** May 6, 2024





## Abstract

To enhance the applicability and measurement accuracy of phase-based optical flow method using complex steerable pyramids in structural displacement measurement engineering applications, an improved method of optimizing parameter settings is proposed. The optimized parameters include the best measurement points of the Region of Interest (ROI) and the levels of pyramid filters. Additionally, to address the issue of updating reference frames in practical applications due to the difficulty in estimating the maximum effective measurement value, a mechanism for dynamically updating reference frames is introduced. Experimental results demonstrate that compared to representative image gradient-based displacement measurement methods, the proposed method exhibits higher measurement accuracy in engineering applications. This provides reliable data support for structural damage identification research based on vibration signals and is expected to broaden the engineering application prospects for structural health monitoring.

## Keywords

Displacement Measurement, Phase-Based Optical Flow, Optimized Parameter Setting

## 1. Introduction

The displacement signals generated during vibrations and dynamic changes are critical data for assessing structural condition and system safety. Traditional contact-based displacement measurement techniques offer high accuracy but can be cumbersome to install and maintain, and their performance may be affected in harsh environments. Non-contact optical measurement techniques,

while highly accurate, have limited measurement ranges. Vision-based displacement measurement techniques enable full-field, efficient, and automated measurements without the need for sensor installation, making them suitable for large structures and complex motions. Therefore, researching vision-based displacement measurement techniques is of significant importance.

Vision-based displacement measurement techniques can be further divided into methods based on image grayscale and methods based on image phase. Grayscale-based visual displacement measurement utilizes variations in the grayscale characteristics of objects in images to infer displacement. This category includes feature point tracking, Digital Image Correlation (DIC), and grayscale-based optical flow methods. These methods find wide applications in structural displacement measurement and structural health monitoring. Cheng *et al.* [1] proposed a method utilizing unmanned aerial vehicles (UAVs) and Digital Image Correlation (DIC) technology for measuring bridge vibrations. Al-Qudah *et al.* [2] proposed an improved Lucas-Kanade (LK) optical flow method for detecting large displacement motions in structures. Dong *et al.* [3] proposed an improved feature matching strategy, where manually crafted descriptors are replaced with learned descriptors from the visual geometry group of Oxford University, aiming to achieve higher precision in structural displacement measurement.

In 1990, Fleet and Jepson [4] first proposed the phase-based optical flow method, which converts a sequence of motion images into a series of spatial domain responses of spatiotemporal velocity-tuned filters. Then, velocity components in each motion direction are computed based on the spatial phase response. Compared to intensity-based optical flow methods, phase-based methods exhibit stronger robustness against interference and greater adaptability to changes in illumination and viewing angles. In 2013, Wadhwa *et al.* [5] introduced the phase-based Eulerian motion magnification method, which significantly enhances the observation of structural dynamic characteristics by amplifying subtle object vibrations. The core of this method lies in using the complex steerable pyramid image decomposition algorithm to obtain phase motion information corresponding to different frequency domain sub-bands of the image, amplifying this phase information proportionally, and then reconstructing the video to achieve motion magnification. In 2015, Chen *et al.* [6] first proposed using the phase-based optical flow with complex steerable pyramids to measure object displacement directly from the phase information of images, and subsequently conducted modal analysis on the measured objects. Since then, the phase-based optical flow with complex steerable pyramids has gained widespread attention. Cosco *et al.* [7] proposed using phase-based motion amplification as a non-destructive testing tool to detect and identify defects in vibrating panels. Sarrafi *et al.* [8] combined phase-based motion estimation and motion amplification methods to estimate damage to wind turbine blades.

To further enhance the performance of the phase-based optical flow method using complex steerable pyramids, Yang *et al.* [9] proposed a steerable pyramid

with sub-pixel compensation for remote measurement and amplification of dynamic vibrations of moving objects. This method employs the steerable pyramid approach to enhance the amplification factor of subtle vibrations with minimal error, thereby suppressing errors introduced during the video stabilization process. Collier *et al.* [10] reconstructed the small motion assumption of phase optical flow for the phase-based optical flow using complex steerable pyramids, aiming to simultaneously extract super-pixel and sub-pixel vibrations. Although many studies have improved the phase-based optical flow method with complex steerable pyramids, determining the optimal pyramid filter levels, selecting the best measurement points, and evaluating the maximum effective measurement value remain unresolved issues in structural displacement measurement scenarios for engineering applications. Addressing these challenges, this paper proposes an improved method of optimizing parameter settings based on the phase-based optical flow method with complex steerable pyramids. These optimized parameters include ROI measurement points and pyramid filter levels. Additionally, the proposed improvement method employs a strategy of dynamically updating reference frames to mitigate the reference frame update issue caused by the inability to determine the maximum effective measurement value.

## 2. The Proposed Method

### 2.1. Overall Framework

The overall framework of the proposed method is illustrated in **Figure 1**.

Firstly, in the initial frame of real structural vibration videos, the ROI is set to ensure that the parameters found in subsequent optimal parameter search steps

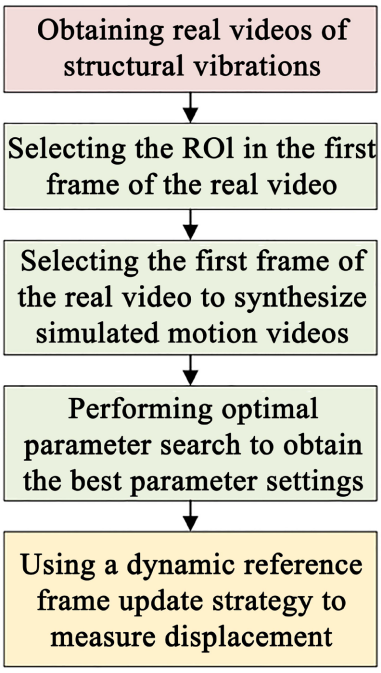


**Figure 1.** The overall framework of the proposed method.

accurately correspond to relevant positions on the structure. Then, the first frame of the real structural vibration video is selected to synthesize simulated motion videos with known displacement values, providing a data basis for subsequent optimal parameter searches. Subsequently, in this simulated motion video, the optimal parameter search method is used to search for the best measurement points in the foreground area of the ROI and find the corresponding optimal filter levels of the complex steerable pyramids. Finally, under the settings of optimal parameters, the phase-based optical flow method is used to measure the structural displacement at the best measurement points of the ROI using a strategy of dynamically updating reference frames. This strategy enables real-time tracking of the structural vibration state and dynamically updates reference frames according to the vibration conditions, ensuring the real-time and accurate measurement results.

## 2.2. Synthesis of Simulated Videos

In engineering applications, real-time measurements in field environments cannot predict the true displacement values of the structure being measured in advance. Therefore, in the proposed method in this paper, the first frame of a real motion video is first used to synthesize a simulated motion video with known displacement values, providing data support for subsequent optimal parameter search steps. When synthesizing the simulated motion video, the sampling frame rate is set to 120, and the sampling time is limited to 0.4 seconds to reduce the computational burden of the optimal parameter search. Considering that the parameters of the best measurement points in the ROI need to adapt to different amplitude displacement changes, two specific time periods are designed in the predefined simulated displacement to simulate different ranges of displacement. The displacement ranges corresponding to these two time periods are between 0 - 1 pixels and 0 - 10 pixels, respectively. Additionally, to simulate the frequency characteristics of real motion, sinusoidal motion at 5 Hz and 9 Hz is superimposed in the first time period, while sinusoidal motion at 9 Hz and 12 Hz is superimposed in the second time period. Through this design, the influence of different displacement amplitudes and motion frequencies on measurement accuracy can be fully considered during the optimal parameter search, ensuring the reliability and effectiveness of the optimal parameter results. The formula for calculating the predefined displacement is as follows:

$$\begin{aligned} s(t) = {} & 5 \times u(t) \times \left[ \sin(2\pi \times 5t) + \sin(2\pi \times 9t) \right] \\ & + 0.5 \times (1 - u(t)) \times \left[ \sin(2\pi \times 9t) + \sin(2\pi \times 12t) \right] \end{aligned} \tag{1}$$

$$u(t) = \begin{cases} 1, t \le 0.2\ \text{s} \\ 0, t > 0.2\ \text{s} \end{cases} \tag{2}$$

After obtaining the predefined simulated displacement, the first frame of the real video is moved using bicubic interpolation to generate the simulated motion video. The formula for bicubic interpolation is as follows:

$$f(x,y)=\sum_{i=0}^{3}\sum_{j=0}^{3} f(x_i,y_j)W(x-x_i)W(y-y_i) \tag{3}$$

where $(x,y)$ is the pixel coordinate after displacement; $(x_i,y_j)$ represents the 16 neighboring points around $(x,y)$ obtained using linear interpolation; $W(x-x_i)$ and $W(y-y_i)$ are the weights of the neighboring points, calculated using the following formula:

$$W(x)=\begin{cases}(a+2)|x|^3-(a+3)|x|^2+1, |x|\le 1\\ a|x|^2-5a|x|^2+8a|x|-4a, 1<|x|<2\\ 0, \text{otherwise}\end{cases} \tag{4}$$

where the value of *a* is −0.5.

### 2.3. The Phase Optical Flow Method Using Complex Steerable Pyramid

After synthesizing the video, it is necessary to search for the optimal algorithm parameter settings for using the phase-based optical flow method with complex steerable pyramids. Therefore, in this section, the principles of the phase-based optical flow method using complex steerable pyramids are introduced. Firstly, the down-sampling rate of the complex steerable pyramid is set to 0, and a set of complex filters with rotation angles of π/2 and 0 of the complex steerable pyramids is used to extract the spatial amplitude and phase information of each frame of the input image sequence:

$$R(x,y,t_j)=A_\theta(x,y,t_j)e^{i\phi_\theta(x,y,t_j)}=(G_\theta+iH_\theta)*I(x,y,t_j)\ \ x,y\in R \tag{5}$$

Among them, $A_\theta(x,y,t_j)$ and $\phi_\theta(x,y,t_j)$ are the amplitude and phase response of the image respectively. In Equation (5), four different types of pyramid level filters, namely Octave, HalfOctave, SmoothHalfOctave, and QuarterOctave, can be chosen to obtain the phase information of the image [11].

According to the assumption of constant phase, the phase of the same pixel remains unchanged in adjacent images:

$$\phi_\theta(x,y,t)=\phi_\theta(x+dx,y+dy,t+dt) \tag{6}$$

The Taylor series expansion of $\phi_\theta(x+dx,y+dy,t+dt)$ at $(x,y,t)$ is carried out, and the first derivative approximation is taken. Equation (6) can be transformed into:

$$\frac{\partial\phi_\theta}{\partial x}dx+\frac{\partial\phi_\theta}{\partial y}dy+\frac{\partial\phi_\theta}{\partial t}dt=0 \tag{7}$$

The gradient of $\phi_\theta(x,y,t)$ at the space coordinate $(x,y)$:

$$\nabla\phi_\theta(x,y,t)=\left(\frac{\partial\phi_\theta}{\partial x},\frac{\partial\phi_\theta}{\partial y}\right)^{\mathrm{T}}=\frac{Im\left[R^*(x,y,t)\nabla R(x,y,t)\right]}{A_\theta^2(x,y,t)} \tag{8}$$

The partial derivative of $\phi_\theta$ to the time variable $\partial\phi_\theta/\partial t$ can be obtained by using the forward difference:

$$\frac{\partial \phi_\theta}{\partial t} = \phi_\theta(x,y,t) - \phi_\theta(x,y,t_j) \tag{9}$$

Assuming that the spatial coordinate is the instantaneous velocity vector of the pixel at $(x,y)$ is $\boldsymbol{v} = (v_x, v_y)^{\mathrm{T}}$, Equation (7) can be transformed into:

$$\frac{\partial \phi_\theta}{\partial x} v_x + \frac{\partial \phi_\theta}{\partial y} v_y + \frac{\partial \phi_\theta}{\partial t} = 0 \tag{10}$$

When the rotation angle is 0, the partial derivative of $\phi_0(x,y,t)$ to the coordinate variable $y$ is 0. When the rotation angle is pi/2, the partial derivative of $\phi_{\pi/2}(x,y,t)$ to the coordinate variable $x$ is 0. Bringing the above conditions into Equation (10) respectively, we can obtain:

$$\boldsymbol{v} = (v_x, v_y)^{\mathrm{T}} = \left( -\left( \frac{\partial \phi_0}{\partial x} \right)^{-1} \frac{\partial \phi_{\pi/2}}{\partial t}, -\left( \frac{\partial \phi_{\pi/2}}{\partial y} \right)^{-1} \frac{\partial \phi_{\pi/2}}{\partial t} \right)^{\mathrm{T}} \tag{11}$$

By multiplying the velocity vector $\boldsymbol{v}$ with the time interval $\Delta t$ of the corresponding two frames, the displacement vector $(x,y)$ of the pixel point at $\boldsymbol{d}$ can be obtained:

$$\boldsymbol{d} = \boldsymbol{v}\Delta t = (d_x, d_y)^{\mathrm{T}} \tag{12}$$

From the above principles, it is understood that since the complex steerable pyramid contains a series of bandpass filters, this method can provide multiple full-field displacement measurements. Therefore, it is necessary to select the optimal filter level and the best measurement points for this method.

## 2.4. Optimal Parameter Search

After obtaining the simulated motion video, the optimal parameter search method is used to obtain the best measurement points within the ROI and the corresponding optimal pyramid filter level parameters, as shown in the overall process in **Figure 2**.

This process consists of two key steps: foreground-background segmentation of the ROI in the first frame of the real motion video and optimal parameter search. The purpose of performing ROI foreground-background segmentation is to filter out the pixel coordinates of the foreground (the structure being measured) within the ROI, ensuring that the best measurement points within the ROI obtained in the subsequent search are located on the structure being measured.

Firstly, the Otsu segmentation algorithm is used to obtain a binary mask image of the foreground ROI. The principle of the Otsu algorithm is to determine the optimal grayscale level segmentation threshold by calculating the maximum inter-class variance between foreground and background. The calculation formula for the grayscale image segmentation threshold $Th$ is:

$$Th = \arg\max_{k \in L} \omega_0 \omega_1 (\mu_0 - \mu_1)^2 \tag{13}$$

where $L$ is the maximum grayscale quantization level of the image, $\mu_0$ and $\mu_1$ are the mean grayscale values of the foreground and background pixels, respectively. Their calculation formulas are:

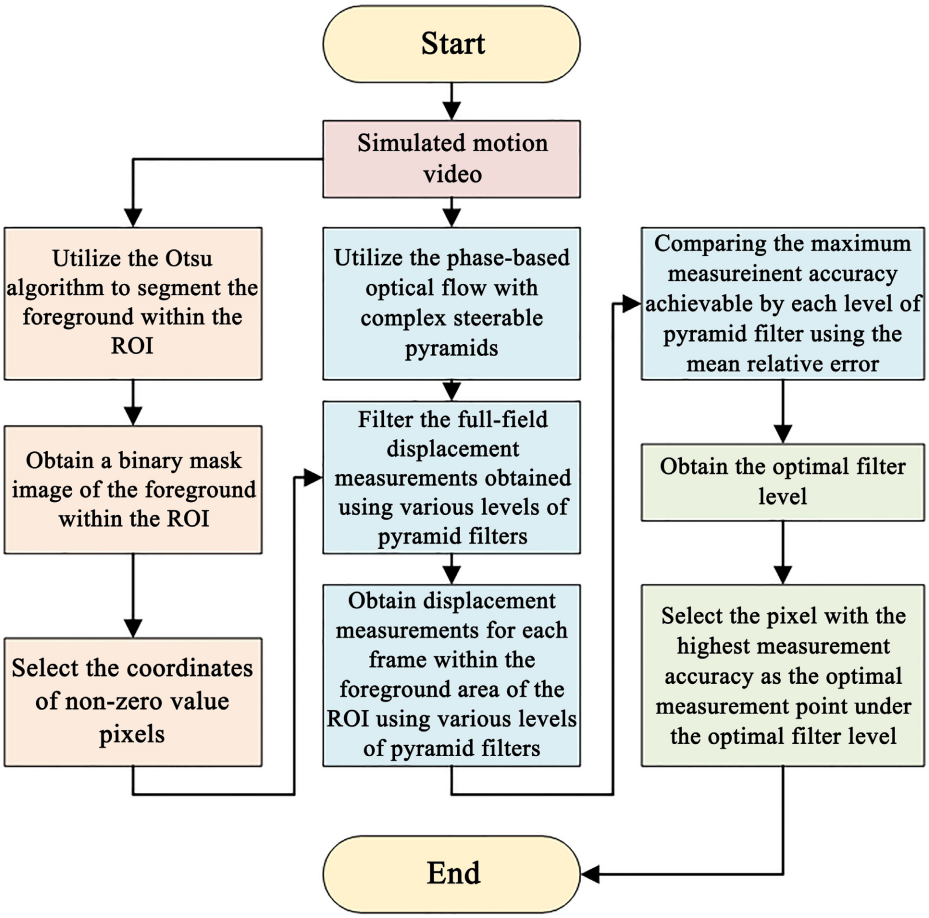


**Figure 2.** Flow chart of optimal parameter search method.

$$u_0 = \sum_{i=0}^{K} \frac{i \times P_i}{\omega_0}, u_1 = \sum_{i=K+1}^{L} \frac{i \times P_i}{\omega_1} \tag{14}$$

where $\omega_0$ and $\omega_1$ are the probabilities of foreground and background pixels, respectively. Their calculation formulas are:

$$\omega_0 = \sum_{i=0}^{K} P_i, \omega_1 = 1 - \omega_0 \tag{15}$$

where $P_i$ is the probability of the grayscale level being *i*. Its calculation formula is:

$$P_i = \frac{n_i}{N}, i = 1, 2, 3, \cdots, K \tag{16}$$

where $n_i$ is the number of pixels with grayscale level *i*, and *N* is the total number of image pixels.

Then, the phase-based optical flow method with complex steerable pyramids is utilized to measure the full-field displacement of each frame image, thus obtaining *P* measurement results of full-field displacement, where the value of *P* is equal to the number of pyramid level filters. Next, based on the coordinates of non-zero pixels in the binary mask image of the foreground ROI, displacement measurement data within the ROI foreground range is accurately filtered. Using

the Mean Absolute Error (MAE) evaluation metric, an analysis is conducted on the precision of displacement measurement for each pixel within the foreground range of P ROIs. The calculation formula is as follows:

$$\mathrm{MAE} = \frac{1}{n}\sum_{i=1}^{n}\left|x_i - y_i\right| \tag{17}$$

where $x_i$ represents the measured displacement value, $y_i$ represents the true displacement, and $n$ represents the number of frames. The measurement accuracy of each pixel in the $P$ foreground regions is calculated individually, and the measurement point with the highest accuracy for each level is selected. Finally, by comparing the accuracy of these $P$ measurement points, the point with the highest accuracy is chosen as the optimal measurement point, and the corresponding level filter is considered as the optimal level filter.

### 2.5. Dynamic Updating of the Reference Frame

After obtaining and setting the optimal parameters for the complex steerable pyramid, the phase-based optical flow method is used to measure the structural displacement at the optimal measurement point within the ROI of the real motion video. As introduced in Section 2.2, the theoretical basis for calculating displacement between two frames using the phase-based optical flow method relies on constant image phase, which requires a short time interval between frames. Therefore, when measuring the vibration displacement of objects in real motion videos, the reference frame is updated every n frames, where n is an interval value set based on the camera's sampling frame rate. Additionally, to address the issue of real-time updating of the reference frame due to the inability to determine the maximum effective measurement value, when measuring the displacement of every n frames, if the measured displacement between the $k$-th frame and the 1st frame in the image block exceeds the maximum displacement set by the simulated motion, the reference frame is updated in place to the $(k-1)$-th frame of the image block.

## 3. Experiment and Analysis

### 3.1. Experimental Setup and Evaluation Metrics

To obtain the experimental data required for this study, a visual vibration measurement experimental platform was constructed, as depicted in **Figure 3**. The experimental setup involves a vibrating speaker with dimensions of 50 mm × 50 mm × 30 mm. The vibration head of the speaker generates vibrations corresponding to the input audio signal. Since the current output from the computer for the sinusoidal vibration audio signal is relatively low, it needs to be amplified by a power amplifier board to drive the vibration head.

A laser displacement sensor (model HEAYI-CL-D1400N) is fixed directly above the vibrating speaker to obtain displacement data in the vertical direction of the vibration head. The sampling frequency of the laser displacement sensor is set to 500 Hz. A data acquisition card (model LINGZHI Electronics DAQ122) is

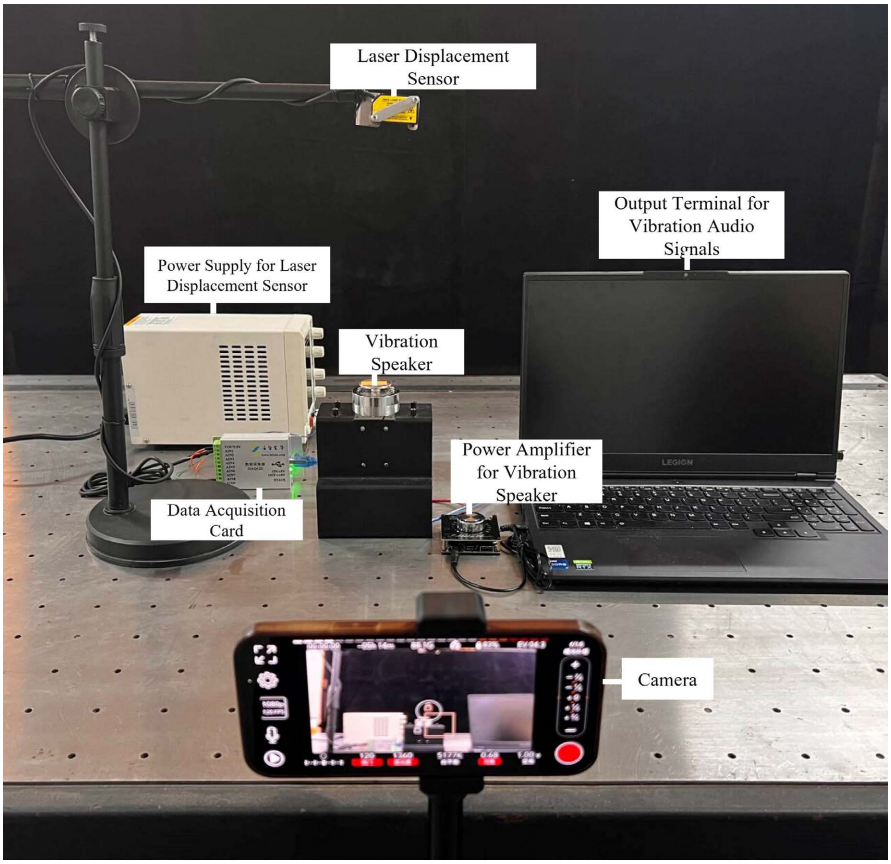


**Figure 3.** Visual vibration measurement experimental platform.

connected to the laser displacement sensor and the computer to read and record the measurement results of the laser displacement sensor in real-time.

Additionally, the camera of an iPhone 13 Pro Max captures the vibration video of the vibration head at a frame rate of 120 frames per second. Before capturing the vibration video with the phone, the "ProMovie" mobile app is used to adjust the camera zoom so that the vibrating speaker occupies most of the central area of the image. The camera focus and sensitivity are then adjusted appropriately to ensure clear imaging of the vibrating speaker in the image. Furthermore, to ensure consistency of parameters during shooting, key camera parameters such as zoom, focus, sensitivity, shutter aperture, and white balance are locked using software before shooting. Since the core of the visual displacement measurement algorithm involves processing grayscale or phase changes between pixels in consecutive frames to obtain displacement, it is essential to keep these parameters constant during shooting to minimize interference with the captured images.

In this paper, a physical-to-image scale conversion factor [12] is utilized to convert the measured pixel displacement into physical displacement. Additionally, four evaluation metrics, namely Root Mean Square Error (RMSE), Normalized Root Mean Square Error (NRMSE), Mean Absolute Error (MAE), and Pearson Correlation Coefficient, are employed to analyze the accuracy of the dis-

placement measurement results.

### 3.2. Comparative Experiments

In the optimal parameter search step proposed in this paper, the Otsu algorithm is utilized to obtain the foreground mask of the first frame ROI of the experimental video and its original ROI image, as shown in Figure 4.

After completing the optimal parameter search step, the optimal filter level parameters obtained on the four pyramids and their corresponding ROI optimal measurement points are shown in Figure 5.

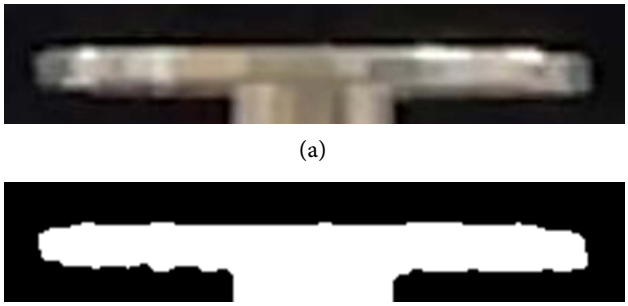

(a)

(b)

Figure 4. The ROI image of the first frame of the experimental vibration video along with its foreground mask: (a) ROI; (b) ROI Foreground Mask Image.

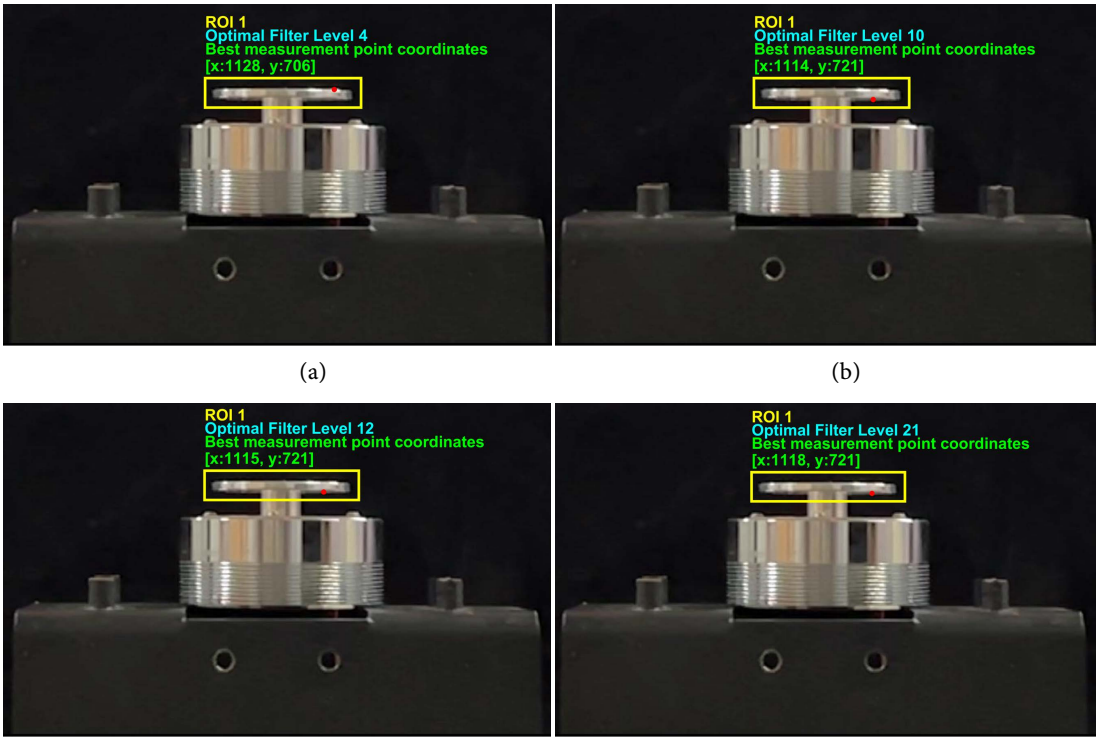


(a) (b)

(c) (d)

Figure 5. The optimal filtering level of the pyramid determined during the search for the best parameters, along with the corresponding optimal measurement points within the ROI: (a) Octave; (b) HalfOctave; (c) SmoothHalfOctave; (d) QuarterOctave.

The results shown in Figure 5 indicate that the proposed method effectively identifies the ROI's optimal measurement point and the corresponding optimal pyramid filter level. Additionally, it's evident from Figure 5 that the optimal filter level and ROI's best measurement point vary across different pyramid types. Therefore, given the diversity of measurement conditions and the complexity of ROI image texture in the tested structures, there is no fixed rule for determining the optimal measurement points for different pyramids.

After obtaining pixel measurement displacements using the method proposed in this paper, the measured pixel displacements are converted to physical displacements using a physical-to-pixel conversion factor (0.4 mm/pixel). Under the optimal parameter settings, when using the four different pyramids, the displacement measurement results at the ROI's optimal measurement points using the method proposed in this paper are illustrated in Figure 6, and the RMSE, NRMSE, MAE, and correlation coefficient, four evaluation metrics of the measurement results, are presented in Table 1.

As demonstrated in Figure 6, regardless of the pyramid type used, the measured vibration signals obtained by the proposed method exhibit high agreement with the true vibration values. However, there is a significant error at the maximum vibration values between the measured signals and the true values. When using the Octave pyramid, the vibration maximum measured by the phase flow method is slightly higher than the true maximum value, whereas with other pyramids, it is slightly lower. Furthermore, it can be observed from the trend of the measurement curves that the results obtained using HalfOctave, SmoothHalfOctave, and QuarterOctave pyramids are quite similar, demonstrating a high level of consistency.

The results shown in Table 1 indicate that compared to other pyramids, the proposed method achieves the lowest RMSE, NRMSE, and MAE for measured displacements when using the SmoothHalfOctave pyramid, with values of 0.046 mm, 0.09, and 0.037 mm, respectively. Therefore, in terms of time-domain evaluation metrics, the proposed method achieves the best overall measurement accuracy when using the SmoothHalfOctave pyramid compared to other pyramids.

To further analyze the accuracy of the measurement results obtained by the proposed method using four different pyramids in the frequency domain, the discrete Fourier transform is applied to obtain the spectra of measured displacements and true displacements, as shown in Figure 7.

Table 1. The accuracy evaluation metrics results obtained using the proposed method for measuring displacement.

| Pyramid type | RMSE (mm) | NRMSE | MAE (mm) | Correlation coefficient |
|---|---|---|---|---|
| Octave | 0.057 | 0.112 | 0.048 | **0.977** |
| HalfOctave | 0.048 | 0.095 | 0.039 | 0.958 |
| SmoothHalfOctave | **0.046** | **0.090** | **0.037** | 0.960 |
| QuarterOctave | 0.048 | 0.094 | 0.039 | 0.963 |

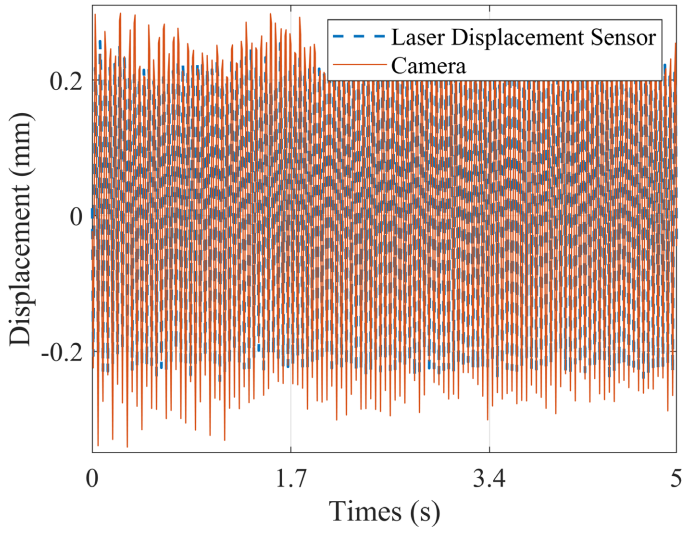
Laser Displacement Sensor
Camera
0.2
0
-0.2
Displacement (mm)
0
1.7
3.4
5
Times (s)

(a)

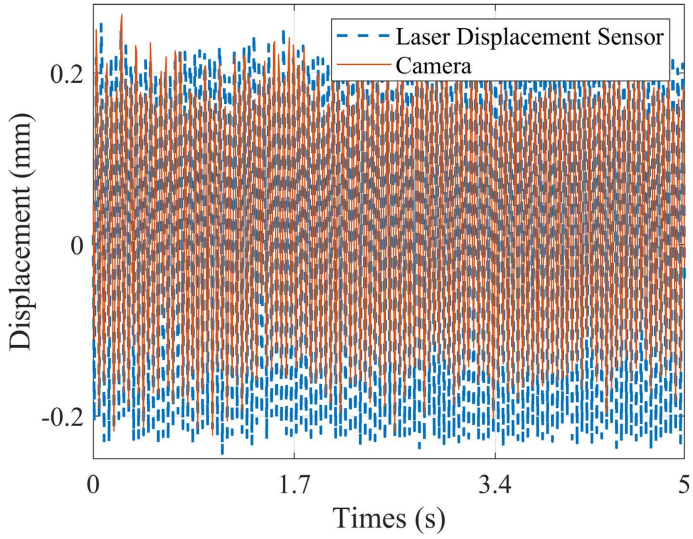
Laser Displacement Sensor
Camera
0.2
0
-0.2
Displacement (mm)
0
1.7
3.4
5
Times (s)

(b)

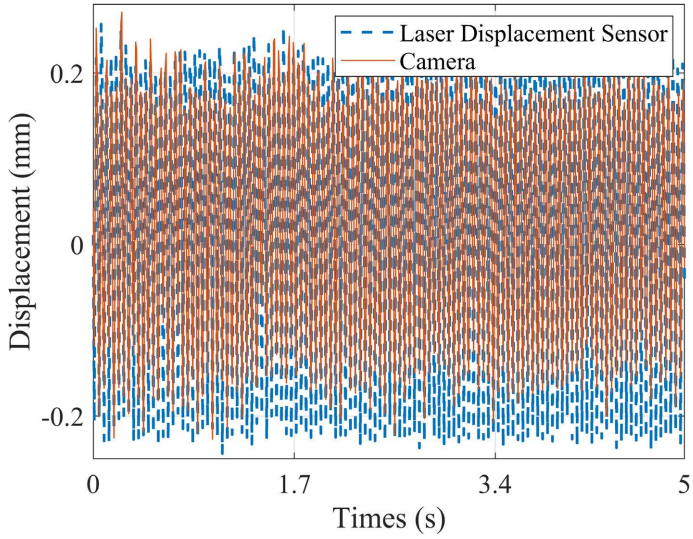
Laser Displacement Sensor
Camera
0.2
0
-0.2
Displacement (mm)
0
1.7
3.4
5
Times (s)

(c)

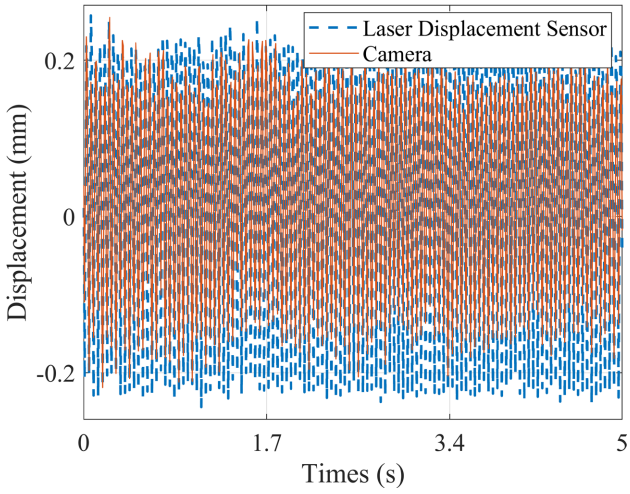


(d)

**Figure 6.** The measured displacement obtained at the optimal measurement point of ROI using the method proposed in this paper: (a) Octave; (b) HalfOctave; (c) SmoothHalfOctave; (d) QuarterOctave.

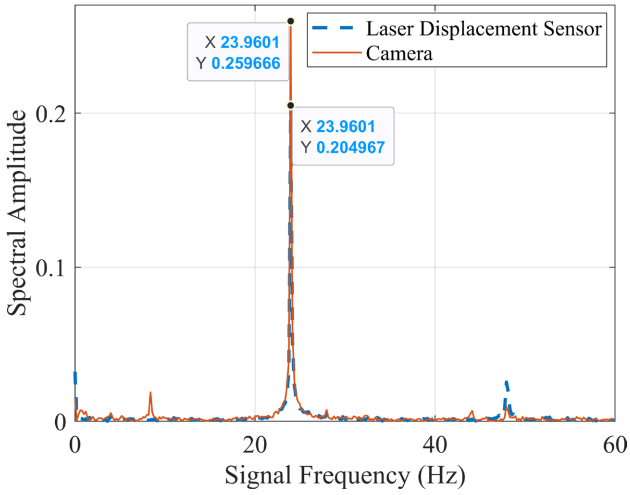


(a)

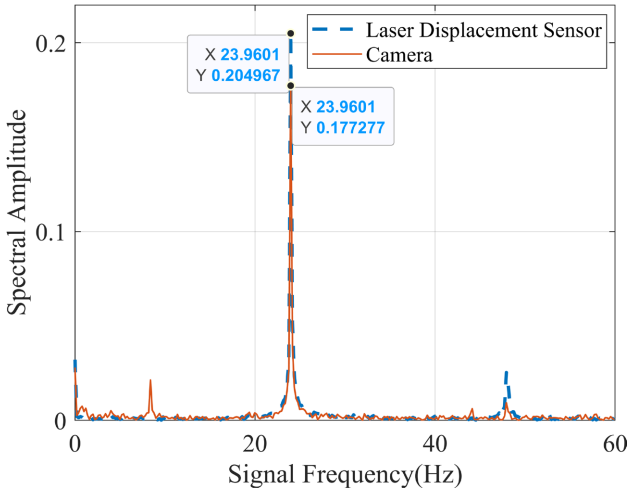


(b)

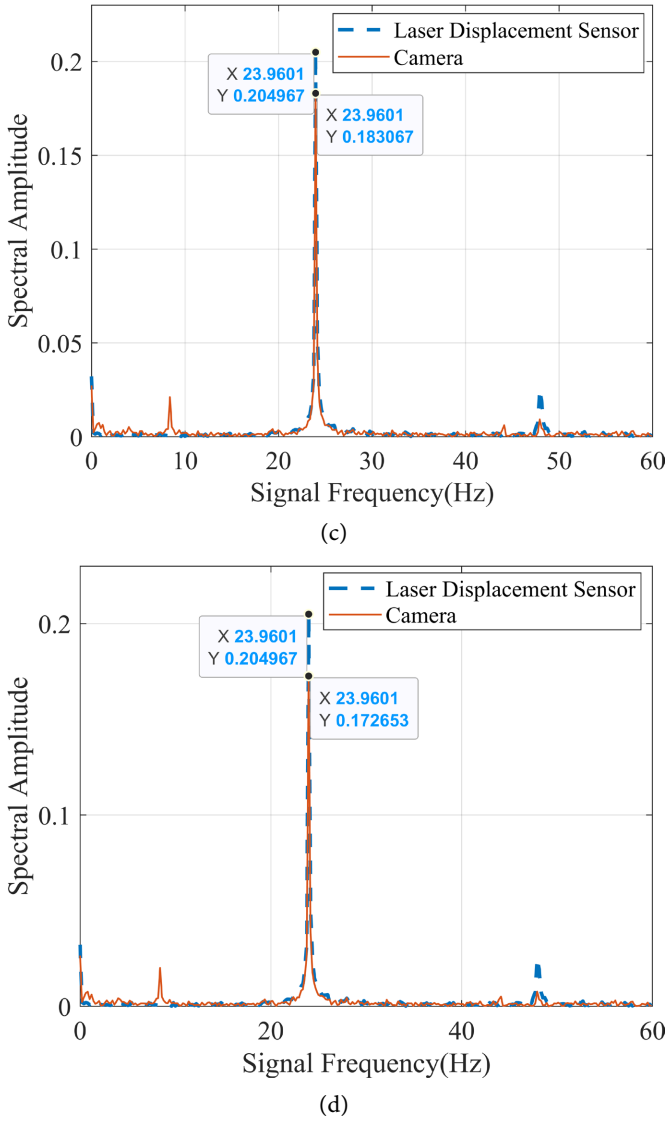


**Figure 7.** The spectrum plots of measured displacement obtained using the proposed method compared to the ground truth displacement: (a) Octave; (b) HalfOctave; (c) SmoothHalfOctave; (d) QuarterOctave.

The results depicted in **Figure 7** demonstrate that the spectra of measured displacements obtained using the four pyramids exhibit high consistency with the true displacements. The errors in peak values of the spectra between the measured displacements and true displacements for the four pyramids are 0.055, 0.028, 0.022, and 0.032, respectively. Therefore, in terms of frequency-domain evaluation metrics, the proposed method achieves the best measurement accuracy when using the SmoothHalfOctave pyramid compared to other pyramids.

In summary, whether in terms of time-domain or frequency-domain metrics, the proposed method achieves the highest measurement accuracy when using the SmoothHalfOctave pyramid. Therefore, for subsequent overall performance evaluations, the proposed method using the SmoothHalfOctave pyramid will be compared with representative visual displacement measurement algorithms.

### 3.3. The Overall Performance Evaluation

Based on the experimental results in Section 3.2, the SmoothHalfOctave pyramid provides the highest displacement measurement accuracy for the method proposed in this paper. Therefore, the method proposed in this paper using the SmoothHalfOctave pyramid is compared with other representative visual displacement measurement methods (Kanade-Lucas-Tomasi (KLT) sparse optical flow [13], Farneback dense optical flow [14], and tracking using SURF feature point matching [15]). When using KLT sparse optical flow and SURF feature point matching, the detection range of feature points is restricted to the ROI region shown in **Figure 5(c)**. Additionally, to achieve optimal tracking performance for KLT sparse optical flow, the quality of Tomasi corners is set to 0.9. Under this setting, only one Tomasi corner is detected within the ROI region. When using SURF feature point matching for tracking, the quality of SURF corners is set to 0.9. Since the number of matched feature points between each video frame and the initial frame is inconsistent, the average measured displacement in the y-direction for all matched points is taken as the displacement for each video frame. When using Farneback dense optical flow, the displacement of the point with the highest accuracy is selected as the final measurement displacement. The displacement measurement results obtained by the aforementioned comparison methods and the method proposed in this paper are shown in **Figure 8**, their displacement measurement accuracy evaluation indicator results are shown in **Table 2**, and their displacement measurement results' spectral information is shown in **Figure 9**.

The results shown in **Figure 8** indicate that the measurement accuracy of KLT sparse optical flow is the poorest, exhibiting an overall downward drift in measured displacement starting from 1.2 seconds. The measured vibration signals obtained using SURF feature point matching and Farneback dense optical flow also exhibit significant errors at signal peaks. Additionally, compared to the displacement ground truth, the measured displacement from SURF feature point matching exhibits a slight time delay, resulting in significant errors in the overall measurement signal. As indicated in **Table 2**, among the comparison methods, Farneback optical flow achieves the highest measurement accuracy, followed by SURF feature point matching, with KLT sparse optical flow being the lowest. These results are consistent with those shown in **Figure 8**.

**Table 2.** Using the comparison method and the method in this paper to obtain the accuracy evaluation index results of the measured vibration signal.

| Method | RMSE (mm) | NRMSE | MAE (mm) | Correlation coefficient |
|---|---|---|---|---|
| KLT Optical Flow | 0.212 | 0.419 | 0.175 | 0.768 |
| Farneback Optical Flow | 0.074 | 0.146 | 0.058 | 0.940 |
| SURF Feature Point Matching | 0.140 | 0.276 | 0.110 | 0.778 |
| Ours | **0.046** | **0.090** | **0.037** | **0.960** |

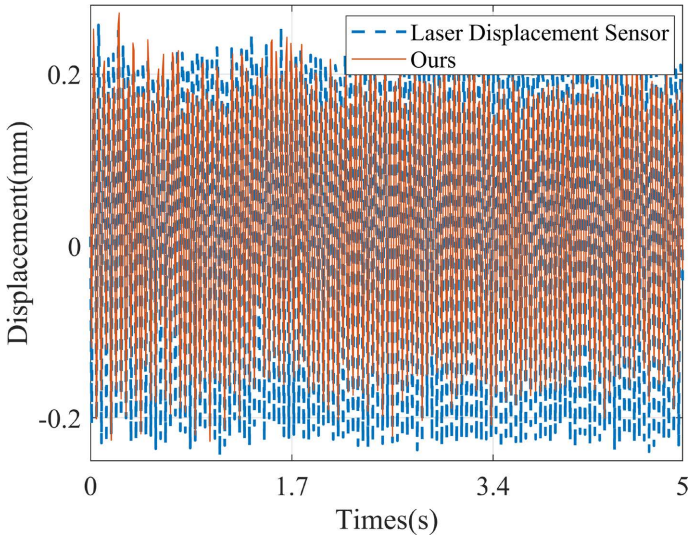
Laser Displacement Sensor
Ours
Displacement(mm)
0.2
0
-0.2
0
1.7
3.4
5
Times(s)

(a)

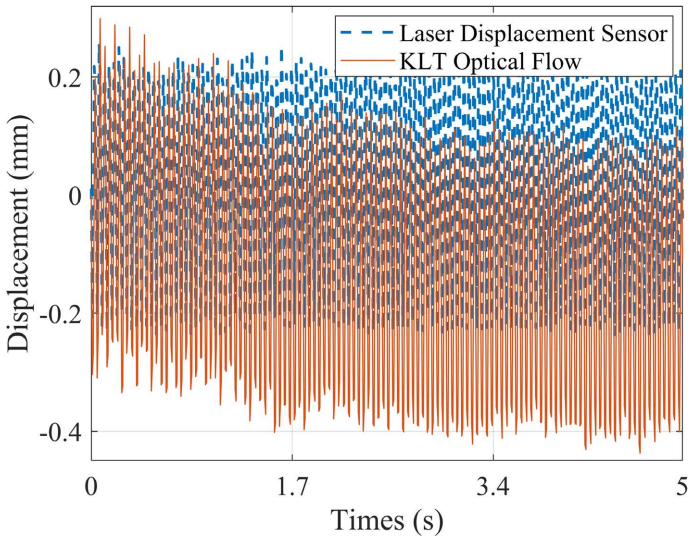
Laser Displacement Sensor
KLT Optical Flow
Displacement (mm)
0.2
0
-0.2
-0.4
0
1.7
3.4
5
Times (s)

(b)

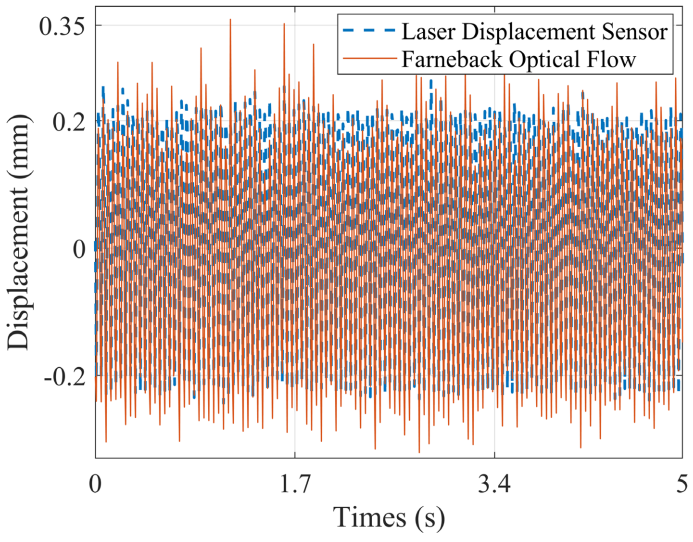
Laser Displacement Sensor
Farneback Optical Flow
Displacement (mm)
0.35
0.2
0
-0.2
0
1.7
3.4
5
Times (s)

(c)

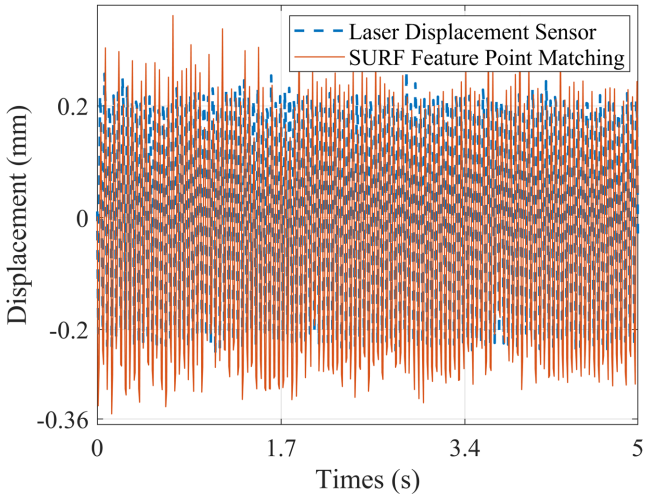


(d)

**Figure 8.** The displacement measurement results obtained using the proposed method and the comparison methods: (a) The proposed method in this paper; (b) KLT Optical Flow; (c) Farneback Optical Flow; (d) SURF Feature Point Matching.

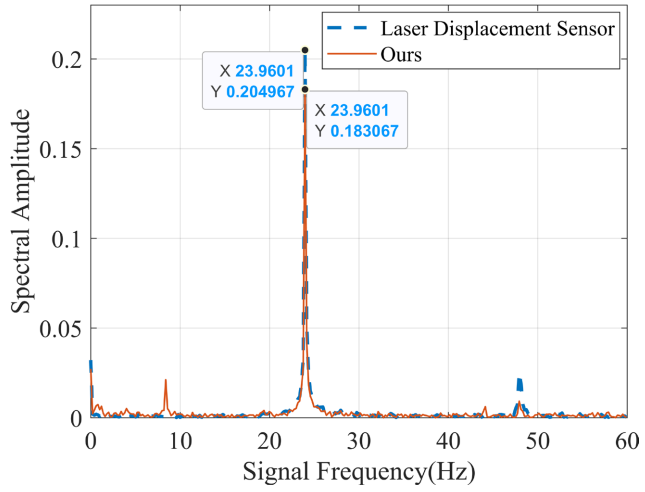


(a)

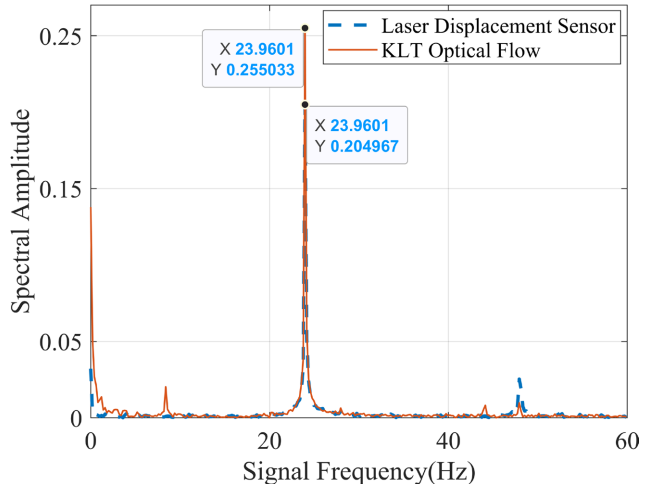


(b)

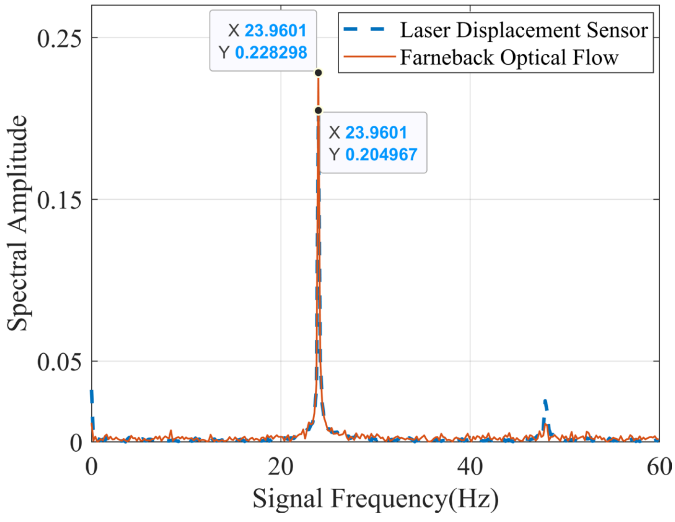


(c)

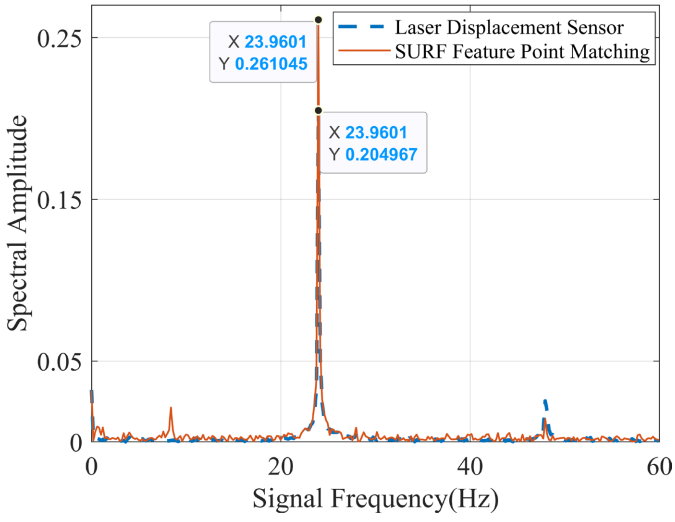


(d)

**Figure 9.** The spectrum of the measured displacement obtained by using the method proposed in this paper and the comparison method: (a) The proposed method in this paper; (b) KLT Optical Flow; (c) Farneback Optical Flow; (d) SURF Feature Point Matching.

Based on the results presented in Table 2, it is evident that compared to the other three contrastive methods, the method proposed in this paper achieves the highest level of accuracy in all temporal indicators. This outcome strongly demonstrates the significant advantages and superiority of the proposed method in terms of displacement measurement accuracy.

From Figure 9, it can be observed that the proposed method and the methods using KLT, Farneback, and SURF obtain measurement errors at the spectral peaks of 0.022, 0.050, 0.023, and 0.056, respectively, compared to the ground truth. The proposed method achieves the highest accuracy in the spectral peak error indicator, indicating excellent performance in spectral parameter measurement.

In conclusion, based on both temporal and spectral evaluation indicators, the proposed method consistently achieves the highest accuracy compared to the comparison methods, demonstrating the superiority of the proposed method in measuring motion parameters and providing a reliable data foundation for subsequent structural damage identification based on vibration signals.

## 4. Conclusion

In response to the limitations of the phase-based optical flow method with the complex wavelet pyramid in practical applications, this paper proposes an enhanced method for optimizing parameter settings. The optimal parameters include the ROI optimal measurement point and the corresponding pyramid filter level. Then, through comparative experiments, the performance of this improved method in displacement measurement when using different pyramids is analyzed. Subsequently, the proposed improvement method is compared with three representative visual displacement measurement methods: KLT sparse optical flow, Farneback dense optical flow, and feature point matching tracking using SURF. The overall performance of the improvement method is evaluated. The experimental results show that, regardless of the time or frequency domain evaluation indicators, compared with representative visual displacement measurement methods, the improved method using the SmoothHalfOctave pyramid achieves the highest measurement accuracy. Its RMSE, NRMSE, MAE, and Pearson correlation coefficient precision evaluation indicators are 0.046 mm, 0.09, 0.037 mm, and 0.96, respectively. Therefore, the proposed improvement method can achieve high-precision structural displacement measurement in practical applications, providing a reliable data basis for subsequent research on structural damage identification based on vibration signals.

## Conflicts of Interest

The authors declare no conflicts of interest regarding the publication of this paper.

## References

[1] Chen, G., Liang, Q., Zhong, W., Gao, X. and Cui, F. (2021) Homography-Based Measurement of Bridge Vibration Using UAV and DIC Method. *Measurement*, **170**, Article ID: 108683. https://doi.org/10.1016/j.measurement.2020.108683

[2] Al-Qudah, S. and Yang, M. (2023) Large Displacement Detection Using Improved Lucas-Kanade Optical Flow. *Sensors*, **23**, Article 3152. https://doi.org/10.3390/s23063152

[3] Dong, C.-Z. and Catbas, F.N. (2019) A Non-Target Structural Displacement Measurement Method Using Advanced Feature Matching Strategy. *Advances in Structural Engineering*, **22**, 3461-3472. https://doi.org/10.1177/1369433219856171

[4] Fleet, D.J. and Jepson, A.D. (1990) Computation of Component Image Velocity from Local Phase Information. *International Journal of Computer Vision*, **5**, 77-104. https://doi.org/10.1007/BF00056772

[5] Wadhwa, N., Rubinstein, M., Durand, F. and Freeman, W.T. (2013) Phase-Based Video Motion Processing. *ACM Transactions on Graphics* (*TOG*), **32**, 1-10. https://doi.org/10.1145/2461912.2461966

[6] Chen, J.G., Wadhwa, N., Cha, Y.-J., Durand, F., Freeman, W.T. and Buyukozturk, O. (2015) Modal Identification of Simple Structures with High-Speed Video Using Motion Magnification. *Journal of Sound and Vibration*, **345**, 58-71. https://doi.org/10.1016/j.jsv.2015.01.024

[7] Cosco, F., Cuenca, J., Desmet, W., Janssens, K. and Mundo, D. (2022) Towards Phase-Based Defect Detection: A Feasibility Study in Vibrating Panels. *Journal of Sound and Vibration*, **537**, Article ID: 117196. https://doi.org/10.1016/j.jsv.2022.117196

[8] Sarrafi, A., Mao, Z., Niezrecki, C. and Poozesh, P. (2018) Vibration-Based Damage Detection in Wind Turbine Blades Using Phase-Based Motion Estimation and Motion Magnification. *Journal of Sound and Vibration*, **421**, 300-318. https://doi.org/10.1016/j.jsv.2018.01.050

[9] Yang, J. and Peter, W.T. (2023) Steerable Pyramid with Subpixel Compensation for Remotely Measuring and Magnifying Dynamic Vibration of Moving Objects. *Measurement*, **211**, Article ID: 112663. https://doi.org/10.1016/j.measurement.2023.112663

[10] Collier, S. and Dare, T. (2023) Informed Pixel Pushing: A New Method of Large-Motion Handling for Phase-Based Optical Flow. *Measurement*, **213**, Article ID: 112711. https://doi.org/10.1016/j.measurement.2023.112711

[11] Wadhwa, N. (2016) Revealing and Analyzing Imperceptible Deviations in Images and Videos. Massachusetts Institute of Technology, Cambridge, MA.

[12] Bhowmick, S., Nagarajaiah, S. and Lai, Z. (2020) Measurement of Full-Field Displacement Time History of a Vibrating Continuous Edge from Video. *Mechanical Systems and Signal Processing*, **144**, Article ID: 106847. https://doi.org/10.1016/j.ymssp.2020.106847

[13] Lee, Y., Lee, G., Moon, D.S. and Yoon, H. (2022) Vision-Based Displacement Measurement Using a Camera Mounted on a Structure with Stationary Background Targets outside the Structure. *Structural Control and Health Monitoring*, **29**, e3095. https://doi.org/10.1002/stc.3095

[14] Yan, W.-J., Feng, Z.-Q., Yang, W. and Yuen, K.-V. (2022) Bayesian Inference for the Dynamic Properties of Long-Span Bridges under Vortex-Induced Vibration with Scanlan's Model and Dense Optical Flow Scheme. *Mechanical Systems and Signal Processing*, **174**, Article ID: 109078. https://doi.org/10.1016/j.ymssp.2022.109078

[15] Colombani, I.A. and Andrawes, B. (2022) A Study of Multi-Target Image-Based Displacement Measurement Approach for Field Testing of Bridges. *Journal of Structural Integrity and Maintenance*, **7**, 207-216. https://doi.org/10.1080/24705314.2022.2088071